A comparative quadrant analysis of turbulence in a plant canopy

Wusi Yue,[1] Charles Meneveau,[2] Marc B. Parlange,[3] Weihong Zhu,[2] René van Hout,[2,4] and Joseph Katz[2]

Received 3 October 2006; revised 28 December 2006; accepted 19 January 2007; published 17 May 2007.

[1] Large-eddy simulation (LES) of turbulence in plant canopies has traditionally been validated using bulk statistical quantities such as mean velocity and variance profiles. However, turbulent exchanges between a plant canopy and the atmosphere are dominated by large-scale coherent structures, and therefore LES must also be validated using statistical tools that are sensitive to details of coherent structures. In this study, LES and measurements using particle image velocimetry (PIV) are compared near the top of the canopy by means of a quadrant-hole analysis of turbulent kinetic energy, vorticity, and dissipation rate. The LES resolves coarse features of individual corn plants and uses the Lagrangian scale-dependent dynamic subgrid model. At the measurement location, there is good agreement between the LES predictions and the field data in terms of most conditionally sampled quantities, confirming the applicability of LES for fundamental studies of vegetation-air interactions and coherent structures. The simulation results confirm that sweeps (the fourth-quadrant events) contribute the largest fraction of turbulent kinetic energy, vorticity, and dissipation rate inside the plant canopy. The magnitudes of the vorticity and dissipation rate at the top of the canopy are highest in the first quadrant (rare events of outward interactions).

Citation: Yue, W., C. Meneveau, M. B. Parlange, W. Zhu, R. van Hout, and J. Katz (2007), A comparative quadrant analysis of turbulence in a plant canopy, *Water Resour. Res.*, *43*, W05422, doi:10.1029/2006WR005583.

1. Introduction

[2] The identification of organized coherent structures in turbulent flows over vegetative canopies has been of primary interest in environmental fluid mechanics for decades, due to the role these structures play in mass and energy exchange. These exchanges are particularly important in land-atmosphere interaction and in riverine and coastal environments [e.g., *Shaw and Schumann*, 1992; *Finnigan and Shaw*, 2000; *Andradottir and Nepf*, 2001; *Ghisalberti and Nepf*, 2004]. Conditional sampling techniques are well established tools for identifying structures that allow specific flow features to be extracted from experimental data. Examples include the detection of turbulent-nonturbulent interfaces [*Sreenivasan et al.*, 1978] and quantification of events associated with turbulent shear layers [*Charnay et al.*, 1976; *Weir and Bradshaw*, 1979]. An early review of applications of conditional sampling in experimental measurements was presented by *Antonia* [1981]. The most frequently used conditional sampling techniques include wavelet analysis [*Meneveau*, 1991; *Farge*, 1992] of coherent structures [*Mahrt*, 1991; *Katul and Parlange*, 1994; *Szilagyi et al.*, 1999; *Marsh et al.*, 2001], quadrant analysis of the Reynolds shear stress [*Willmarth and Lu*, 1972; *Wallace et al.*, 1972; *Priyadarshana and Klewicki*, 2004; *Aubertine and Eaton*, 2005] and heat flux [*Shen and Leclerc*, 1997; *Su et al.*, 1998; *Cava et al.*, 2006], and variable interval time averaging (VITA) technique [*Blackwelder and Kaplan*, 1976; *Alfredsson and Johansson*, 1984; *Porporato*, 1999; *Mokhtarzadeh-Dehghan and Yuan*, 2002]. Originally devised for experimental data analysis, these techniques were later applied to numerical simulations, e.g. quadrant analysis on atmospheric flow by large-eddy simulation (LES) [*Kim et al.*, 2003], VITA analysis on channel flow by direct numerical simulation [*Chu and Karniadakis*, 1993], and wavelet analysis of canopy flow by LES [*Watanabe*, 2004].

[3] In quadrant analysis [*Lu and Willmarth*, 1973], the shear stress is decomposed into four quadrant events. The events in quadrant 2 and 4 contribute positively to the downward momentum flux, and are usually called ejections and sweeps, respectively. These events are involved in turbulence near-wall bursting [*Robinson*, 1991]. The quadrant analysis has mostly been applied to smooth wall turbulent boundary layers, but also to canopy turbulent flows, e.g., wheat canopy [*Finnigan*, 1979], corn canopy [*Shaw et al.*, 1983], wind tunnel

[1]Department of Geography and Environmental Engineering and Center for Environmental and Applied Fluid Mechanics, Johns Hopkins University, Baltimore, Maryland, USA.
[2]Department of Mechanical Engineering and Center for Environmental and Applied Fluid Mechanics, Johns Hopkins University, Baltimore, Maryland, USA.
[3]School of Architecture, Civil and Environmental Engineering, Ecole Polytechnique Federale de Lausanne, Lausanne, Switzerland.
[4]Now at Faculty of Mechanical Engineering, Technion–Israel Institute of Technology, Technion City, Haifa, Israel.

0043-1397/07/2006WR005583$09.00

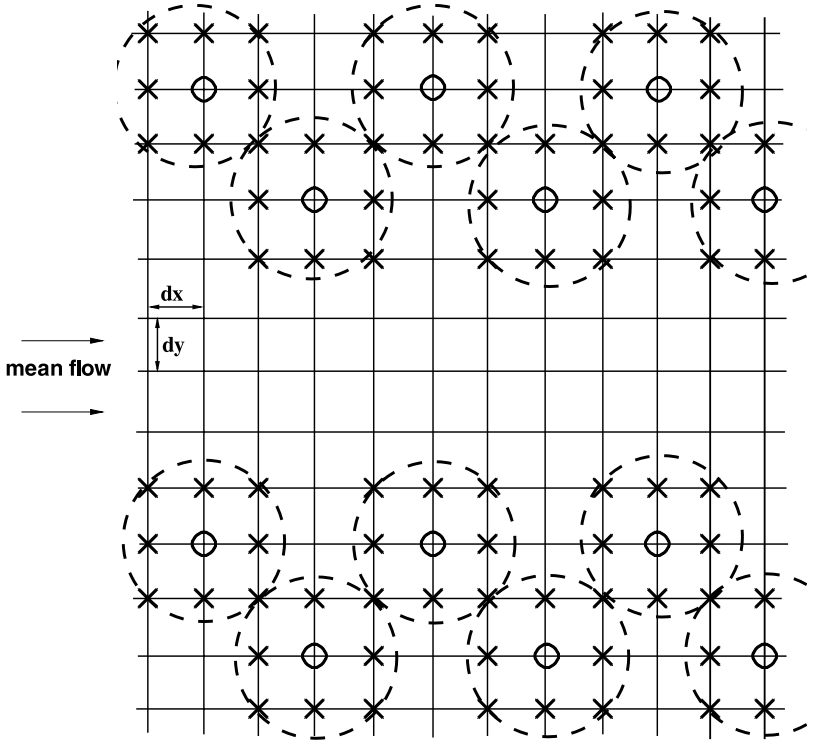

Figure 1. Computational grid and plant-scale representation of corn plants. Solid circles mark stems, crosses mark leaves, and big dashed circles enclose individual plants.

models [*Raupach et al.*, 1986], water flume model [*Poggi et al.*, 2004a], and forests [*Baldocchi and Meyers*, 1988; *Gardiner*, 1994]. Canopy turbulence is characterized by the absorption of momentum through the aerodynamic drag of foliage and the high turbulence intermittency within the canopy, as reviewed by *Raupach and Thom* [1981] and *Finnigan* [2000]. The quadrant analysis of canopy turbulence consistently reveals that sweeps are the primary contributors to downward momentum transfer within the canopy, implying that the canopy is penetrated by fast moving downward gusts. This is in contrast to what is observed in smooth wall boundary layers where ejections are the major contributors near the wall (beyond the buffer layer), but in agreement with the results in rough wall boundary layers where sweeps start to dominate as the distance to the wall is decreased [*Raupach*, 1981; *Raupach et al.*, 1991]. In a water flume experiment, *Katul et al.* [2006], however, found that ejections slightly dominate the momentum transfer within sparse canopies.

[4] *Shen and Leclerc* [1997] and *Su et al.* [1998] conducted quadrant analysis of turbulence structures in LES models of forest canopies. *Shen and Leclerc* [1997] focused on the shear stress and heat flux analysis in unstable conditions. They found that under stronger unstable conditions, contributions from ejections increase and those from sweeps decrease. *Su et al.* [1998] carried out analysis of LES data for momentum flux, scalar flux, and event duration in neutrally stratified flow and compared the results with experimental data. They found that inside the canopy, sweeps occupy less of the overall time than ejections, but make a larger contribution to momentum flux than ejections. They also showed that total stress and duration decrease significantly along with quadrant hole size (excluded region in (u', w') plane). Quadrant analysis results from a recent field experiment study in a corn field were presented by *Zhu et al.* [2007]. Although quadrant analysis is traditionally performed for conditional sampling of the Reynolds shear stress and turbulent heat flux, *Zhu et al.* [2007] extended the technique to include more general properties of turbulence in plant canopy flows, e.g., turbulent kinetic energy, vorticity,

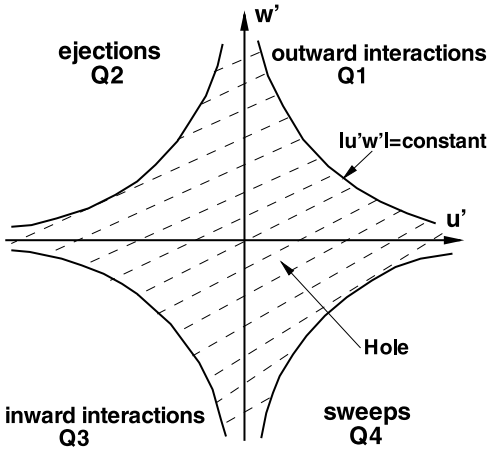

Figure 2. Schematic of quadrant events and "hole" region.

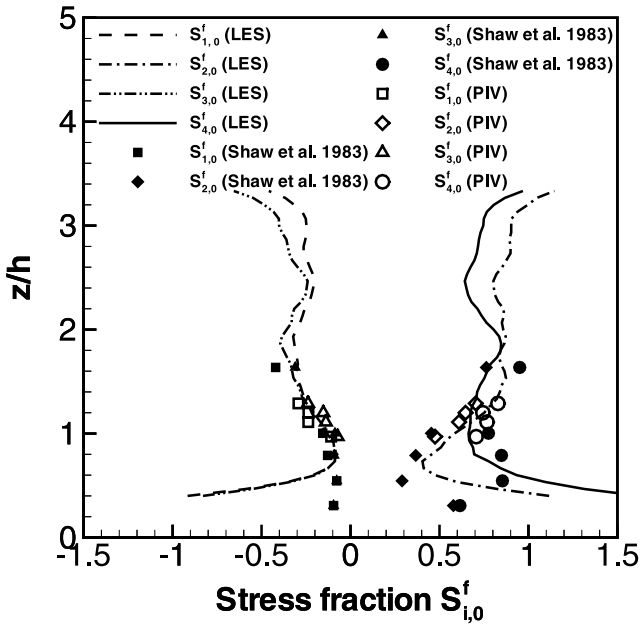

Figure 3. Stress fractions contributed by each quadrant as a function of normalized height z/h, where h is the height of the canopy.

and dissipation rate. The dissipation rate and vorticity are properties of small-scale motions while the momentum flux is representative of larger scales. Turbulent kinetic energy (TKE) is also dominated by contributions from the large scales. The actual property magnitudes and their corresponding durations are examined to provide a measure of the strength of the conditionally sampled signals. The main objective of the present paper is to make a detailed comparison between PIV data observed in the corn field and LES, with a focus on the quadrant-hole analysis tools. In particular, we want to compare the LES results with the PIV data in the quadrant-hole map for each separate event, looking at the duration and large-scale quantities of shear stress and TKE, as well as small-scale quantities of dissipation and vorticity. The computational data are obtained from an LES of the corn canopy that resolves coarse features of individual corn plants and uses the Lagrangian, scale-dependent dynamic subgrid model [*Yue et al.*, 2007]. The field data are obtained using particle image velocimetry (PIV) [*van Hout et al.*, 2007]. One of the main objectives is to test whether LES confirms field observations that sweeps dominate within the canopy, and that the magnitudes of the vorticity (at the LES/measurement resolution) and dissipation rate are highest in the first quadrant. This should allow a further assessment of the usefulness of LES to accurately simulate flows in plant canopies. Section 2 briefly describes the LES and the field experiment. Section 3 outlines the parameters used in the quadrant analysis of turbulence structures in the corn canopy. Section 4 presents the quadrant fraction results of LES and the comparison with PIV. Section 5 presents the quadrant magnitude results based on time duration of the events for both the LES and PIV. Finally in section 6, we summarize the results and provide conclusions.

2. Brief Description of Numerical Simulation and Field Experiment in Corn Canopy

[5] A fully matured corn field with an average canopy height of 2.67 m is numerically and experimentally studied with LES and PIV. The corn field was planted in a dense arrangement, characterized with a leaf area index of 6.0 ± 0.6 and a projected frontal area index of 3.7 ± 0.5 [*van Hout et al.*, 2007]. The LES employs a plant-scale approach that resolves the plant arrangement and coarse features of individual corn plants, including an equivalent leaf area index of 6.0 (for details, see *Yue et al.* [2007]). An individual corn plant is modeled as a force cylinder, with the central grid point resisting the flow with cylindrical drag and the surrounding eight horizontal grid points applied with leaf drag. This is different from previous numerical simulations that treated

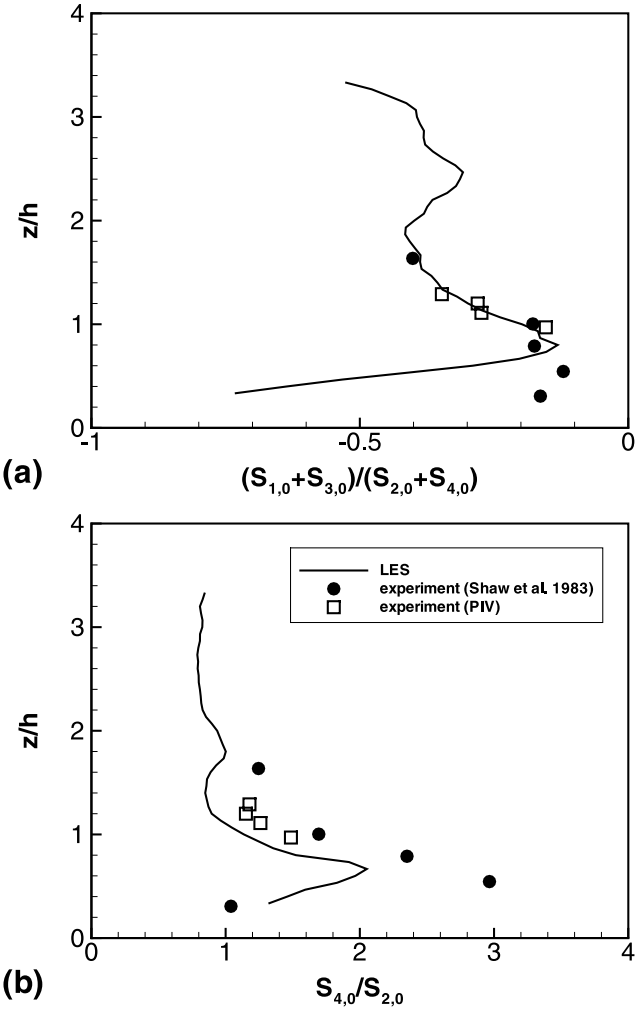

Figure 4. Event ratios as a function of normalized height. (a) Ratio of negative to positive contributions to the momentum flux; (b) ratio of sweeps to ejections.

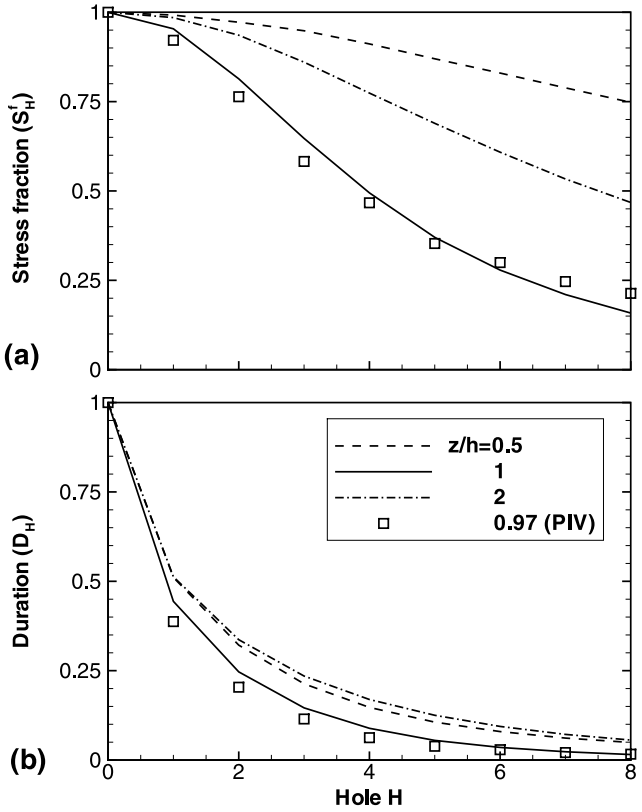

Figure 5. The sum of all four quadrant fractions with an excluded varying hole size. (a) Stress; (b) duration.

the canopy field as a porous body of horizontally uniform area density, called the field-scale approach by *Yue et al.* [2007]. Figure 1 shows the computational grid in the horizontal plane below the canopy top for the plant-scale approach, where the circle symbols represent the position of plant stems (modeled using drag coefficient appropriate for a cylinder in cross flow) and the cross symbols represent the plant leaves (modeled with leaf drag). The computational domain is $L_x : L_y : L_z = 4.5\ h : 2.4\ h : 3.9\ h$, where h is the corn canopy height, with respective grid resolution of $N_x : N_y : N_z = 160 : 64 : 60$. Uniform grid spacings are used in each direction. Periodic boundary conditions are used in horizontal directions. The bottom boundary uses a standard imposed stress approach based on the equilibrium law of the wall [*Mason*, 1994; *Bou-Zeid et al.*, 2005]. The filtered incompressible Navier-Stokes equations are solved by applying a pseudospectral method in the horizontal directions and centered finite difference method in the vertical direction [*Albertson and Parlange*, 1999a, 1999b; *Porté-Agel et al.*, 2000]. The vertical velocity component w is staggered with horizontal components u and v. The convective terms are dealiased by padding and truncation using the 3/2 rule [*Orszag*, 1970]. A scale-dependent dynamic Lagrangian model is employed to model the unresolved subgrid-scale stress [*Bou-Zeid et al.*, 2004, 2005]. A time series (5000 samples separated by 4.2×10^{-3} s) of the velocity fluctuation field in a vertical plane of (x, z) set in the middle of the two corn plant rows is stored for the quadrant analysis presented here.

[6] The PIV measurements were obtained on 22 July 2003 [*van Hout et al.*, 2007]. The laser sheet and CCD camera were mounted on a retractable and rotatable platform. The plane of the laser sheet was aligned with the wind direction using a wind vane. The camera has a field of view of 18.2×18.2 cm^2. The measurements were performed at 4 different elevations, $z/h = 0.97$, 1.11, 1.20, and 1.29, where z is the vertical distance from the ground and h is the average canopy height. At each elevation, 4096 double-exposure images were recorded at an acquisition rate of 4 Hz. Only the experimental data at $z/h = 0.97$ are used in this paper for comparison with the LES generated velocity fields.

3. Definition of Parameters in Quadrant-Hole Analysis

[7] The quadrant-hole analysis first introduced by *Lu and Willmarth* [1973] has been often used to investigate turbulence structures. In this technique, the velocity fluctuations are decomposed into four quadrant domains with the relative quiescent motion excluded from the domain. The first quadrant events ($u' > 0$, $w' > 0$) are "outward interactions," the second quadrant events ($u' < 0$, $w' > 0$) are "ejections," the third quadrant events ($u' < 0$, $w' < 0$) are "inward interactions," and the fourth quadrant events ($u' > 0$, $w' < 0$) are "sweeps." In the present paper we follow the common practice of referring to parts of the signal identified by the above criteria as "events" [*Wallace et al.*, 1972; *Lu and Willmarth*, 1973; *Raupach*, 1981]. It is important to recall, however, that this is not necessarily equivalent to the notion of a particular "coherent structure", which requires the more complete characterization of an entire three-dimensional fluid packet.

[8] By identifying a hyperbolic region in the (u', w') plane, relative quiescent motions can be excluded in the quadrant analysis [*Lu and Willmarth*, 1973]. The hole size H associated with the excluded region (see Figure 2) is defined as

$$H = |u'w'|/|\overline{u'w'}| \tag{1}$$

where the overbar denotes time averaging. Note that the above definition of the hole size H differs from the original definition of *Lu and Willmarth* [1973] since it uses the mean stress value instead of the RMS velocity values for normalization. A mean quadrant event, as a function of H, such as the Reynolds shear stress (negative momentum flux) $\overline{u'w'}_{i,H}$, denoted as $S_{i,H}$, is defined as

$$S_{i,H} = \frac{1}{T}\int_0^T u'(x,z,t)w'(x,z,t)I_{i,H,t}(u',w')dt \tag{2}$$

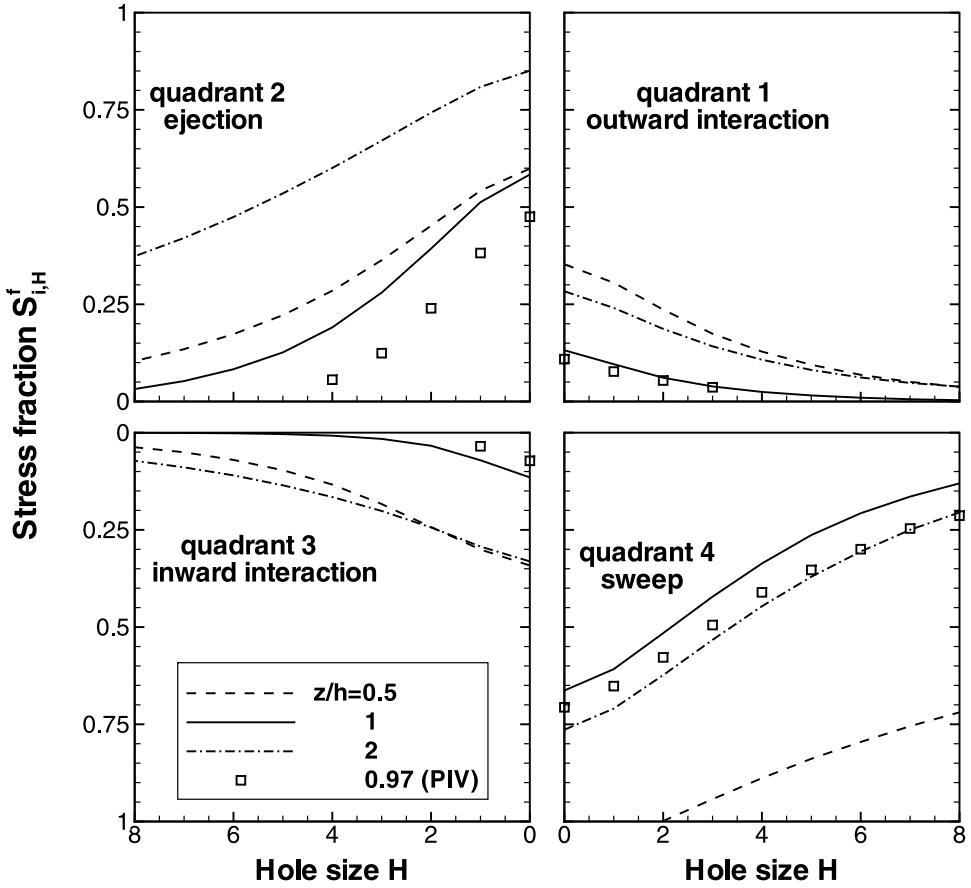

Figure 6. Stress fractions $S^f_{i,H}$ at three elevations z/h = 0.5, 1, and 2. The PIV data are at z/h = 0.97.

where i indicates a specific quadrant. In this formulation, t is time and T and is the sampling time period, and x and z are the streamwise and vertical coordinates, respectively. $I_{i,H,t}$ is a conditional sampling function defined as

$$I_{i,H,t}(u',w') = \begin{cases} 1, & \text{if } (u',w') \text{ is in quadrant } i \\ & \text{and } |u'w'| \geq H|\overline{u'w'}| \\ 0, & \text{otherwise} \end{cases} \quad (3)$$

The quadrant fraction of the stress $S^f_{i,H}$ is

$$S^f_{i,H} = S_{i,H}/S \quad (4)$$

where S is the mean stress,

$$S = \frac{1}{T}\int_0^T u'(x,z,t)w'(x,z,t)dt \quad (5)$$

and the obtained time-averaged $S_{i,H}$ and S are then averaged over the streamwise direction in LES. All the subsequent quantities are averaged over the streamwise direction as well, to enhance statistical convergence. It is clear that

$$\sum_{i=1}^{4} S^f_{i,0} = 1 \quad (6)$$

since the hole region vanishes at $H = 0$. The above technique is also applied to the turbulent kinetic energy K, the magnitude of spanwise fluctuating vorticity $\omega'_y = \sqrt{(\partial u'/\partial z - \partial w'/\partial x)^2}$, and the dissipation rate ϵ. For instance, the vorticity fraction $\omega^f_{i,H}$ is computed as

$$\omega^f_{i,H} = \omega_{i,H}/\omega \quad (7)$$

where

$$\omega_{i,H} = \frac{1}{T}\int_0^T \omega'_y(x,z,t)I_{i,H,t}(u',w')dt \quad (8)$$

$$\omega = \frac{1}{T}\int_0^T \omega'_y dt, \quad (9)$$

and $K^f_{i,H}$ (TKE fraction) and $\epsilon^f_{i,H}$ (dissipation fraction) are calculated using the same formulation.

[9] In order to assess the strength of event signals, the duration of the events is also computed,

$$D_{i,H} = \frac{1}{T}\int_0^T I_{i,H,t}dt. \quad (10)$$

The quadrant fractions described above do not take into account the event duration; hence we do not know the signal magnitude of the different quadrant events. The normalized

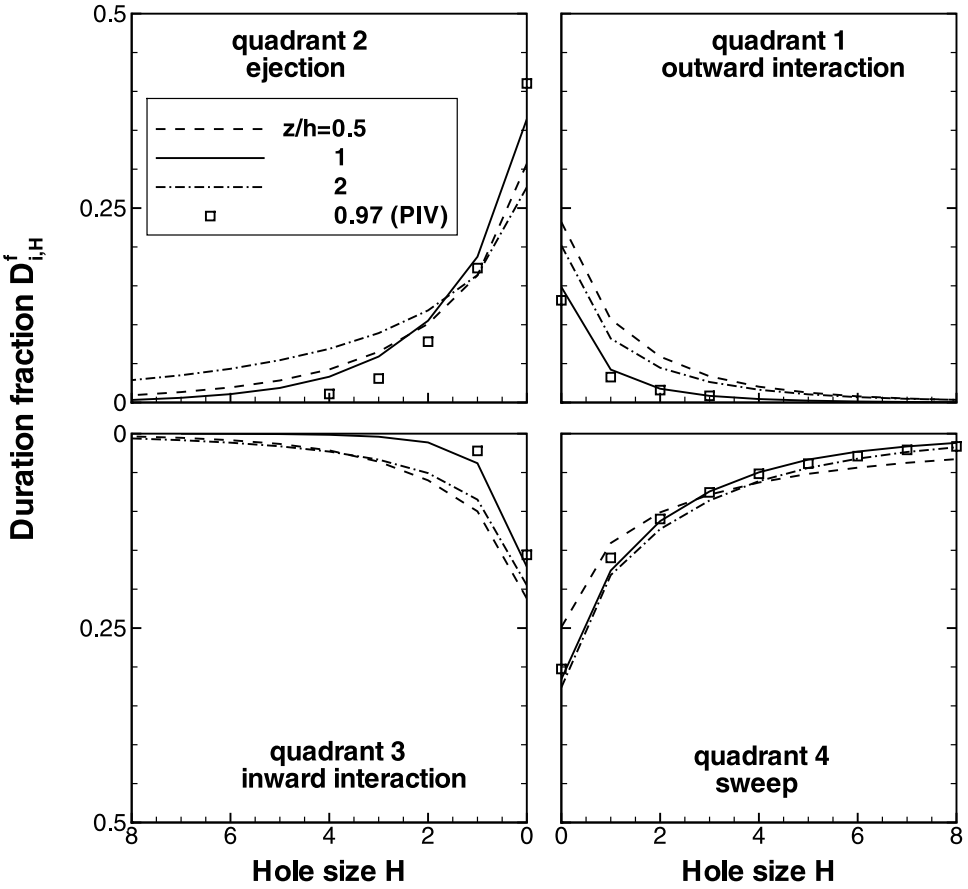

Figure 7. Duration fractions $D^f_{i,H}$ at three elevations z/h = 0.5, 1, and 2. The PIV data are at z/h = 0.97.

magnitude of a quadrant event taking into account the event duration, for example, the shear stress, is determined as follows:

$$S^D_{i,H} = \frac{S_{i,H}}{D_{i,H} S}. \tag{11}$$

This is the normalized average signal strength and provides a measure of the strength of event signals in comparison to the event fraction. TKE magnitude ($K^D_{i,H}$), vorticity magnitude ($\omega^D_{i,H}$), and dissipation magnitude ($\epsilon^D_{i,H}$) are calculated in the same way, e.g.,

$$\omega^D_{i,H} = \frac{\omega_{i,H}}{D_{i,H} \omega}. \tag{12}$$

4. Quadrant Fractions

4.1. Shear Stress and Duration

[10] The quadrant stress fractions and ratios as a function of normalized height z/h are illustrated in Figures 3 and 4, where h is the height of the canopy, without the quadrant hole excluded from the quadrant map. Figure 3 shows the stress fractions contributed by each quadrant. The agreement between the LES data and the experimental data of *Zhu et al.* [2007] and *Shaw et al.* [1983] is good except near the ground where the magnitude of the stress is very small and a large number of samples are needed to accurately calculate the event fractions. Some discrepancy may be due to different conditions in the two corn fields, such as leaf area index. Note that *Poggi et al.* [2004b] found that sweeps become stronger within denser canopies and ejections become stronger within sparser canopies. Above the canopy height, the fractions of $S^f_{1,0}$ (outward interactions) and $S^f_{3,0}$ (inward interactions) are both smaller than 0.5 above the canopy height while those of $S^f_{2,0}$ (ejections) and $S^f_{4,0}$ (sweeps) are both larger than 0.5. Within the canopy, sweeps have the largest fraction. Above the canopy, however, ejections have the greatest fraction of stress. These results are in agreement with previous research in canopy flows. Figure 4a shows the ratio of the upward and downward components, $(S_{1,0} + S_{3,0})/(S_{2,0} + S_{4,0})$, called the exuberance ratio by *Shaw et al.* [1983]. The LES prediction of this ratio agrees well with the experimental data except near the ground, possibly due to the same reason as above. The two interactions reach 42% of the positive quadrant events around z/h = 2 and then decrease at higher elevation. The anomalies near the top boundary may be caused by the limited sample size and the very small shear stress. Figure 4b shows the ratio of sweeps to ejections. It is evident that the ratio is nearly a constant 0.8 above the canopy in the LES prediction. Within the canopy, sweeps are much larger than ejections, indicating gust dominated motion inside the canopy. The LES prediction shows a maximum ratio of 2 around z/h = 0.6, while the experimental data of *Shaw et al.* [1983] show a maximum value

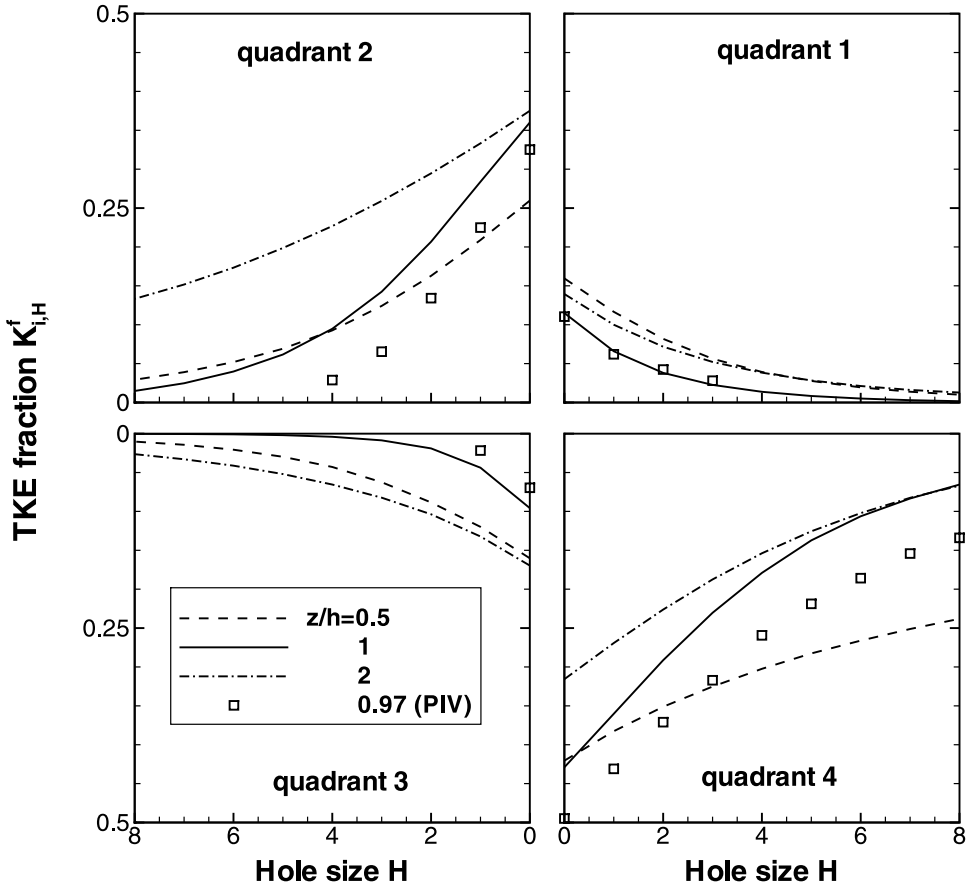

Figure 8. Turbulence kinetic energy (TKE) fractions $K^f_{i,H}$ at three elevations z/h = 0.5, 1, and 2. The PIV data are at z/h = 0.97.

of 3. This difference may be due to the fact that the simulated corn canopy has a higher leaf area index than *Shaw et al.* [1983], increasing damping of the sweeps.

[11] Figure 5a shows the stress fraction S^f_H (sum of the four quadrant fractions) against the hole size H at three elevations z/h = 0.5, 1, and 2. The LES predictions at the canopy top agree very well with the PIV data. The stress fraction decreases most quickly with the hole size at the canopy top and slowest inside the canopy. This suggests that there are some relatively large magnitude quadrant events occurring inside the canopy (mostly the sweeps as shown in Figure 6), although the total shear stress is the largest at the canopy top [*Yue et al.*, 2007]. At the canopy top, about 50% of the stress is from the large magnitude events (H = 4), and above the canopy (z/h = 2) the same percentage of the stress is from even stronger events (H = 8). Inside the canopy, occasionally 75% of the stress is from events above H = 8, attributed to a strong gust inside the canopy. Figure 5b shows the duration D_H against the hole size at the three elevations. The durations at the three elevations drop at almost the same rate along with H. At H = 4, the duration is only 10% of that at the canopy top, indicating that one half of the stress is due to the events occurring 10% of the time. Very similar results were reported by *Shaw et al.* [1983], demonstrating that much of the momentum flux is transported during periods of strong turbulence activity occurring over short duration of time.

[12] The quadrant stress fractions at the three elevations are shown in Figure 6. LES predicts the same quadrant event trends at the canopy top as in PIV. The LES predictions of ejections at the canopy top are higher than the PIV data, and lower for sweeps. This difference may be caused by the shear-free upper boundary imposed in the LES. It prevents eddies from crossing the upper boundary of the limited computational domain, which inhibits large eddies sweeping from the upper part of the atmospheric boundary layer. Sweeps contribute the most at any hole size at and below the canopy top, especially within the canopy (z/h = 0.5) where sweeps contribute 70% and more for $H \leq 8$. Above the canopy (z/h = 2), ejections contribute the most. Even for H = 8, the contribution from ejections is 37.5% and that of sweeps only 20%. Outward and inward interactions have negative contributions of less than 10% each. These two interactions have lower fractions at the canopy top than at any other elevation, indicating that momentum transfer is most efficient at the canopy top. In contrast to ejections and sweeps, the two interactions show no significant fraction difference inside (z/h = 0.5) and above (z/h = 2) the canopy.

[13] In Figure 7, the quadrant duration fractions are presented. The agreement between LES and PIV at the canopy top is excellent. The durations are not significantly dependent on the elevation. Ejections and sweeps are the dominant events, and sweeps are observed to slightly dominate at the large hole size (H > 4). The inward and

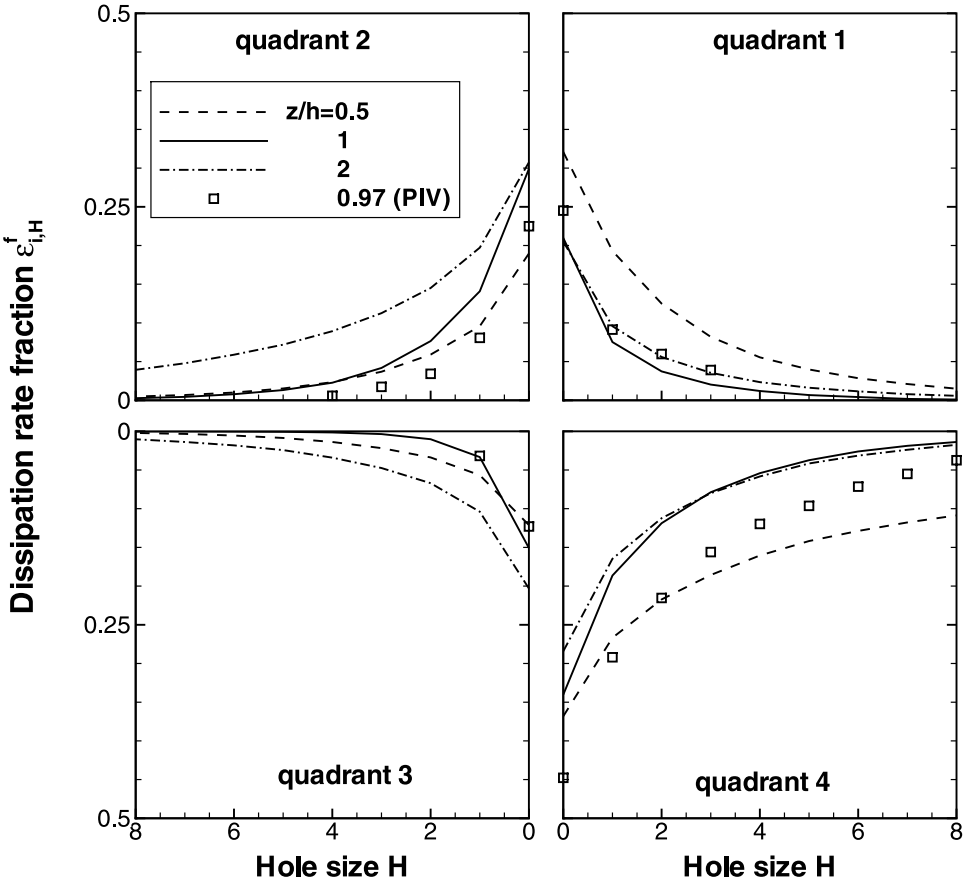

Figure 9. Dissipation rate fractions $\varepsilon^f_{i,H}$ at three elevations $z/h = 0.5$, 1, and 2. The PIV data are at $z/h = 0.97$.

outward interactions cease after $H = 5$. Figure 7 suggests that the reason why the stress fractions of outward and inward interactions are smaller than those of ejections and sweeps is not necessarily due to the weaker signals (smaller magnitudes) but possibly the short duration of the two interactions.

4.2. Turbulent Kinetic Energy, Dissipation Rate, and Vorticity

[14] The quadrant TKE fractions are plotted in Figure 8. In order to compare the LES predictions with the PIV measurements, only the streamwise and vertical components are included, i.e., $\overline{u'^2} + \overline{w'^2}$. The LES predictions of the fraction of ejections at the canopy top are higher than the PIV data, and lower for the sweeps, although the sum is in quite good agreement (not shown here). The difference may be caused by the top boundary conditions imposed in the LES, as discussed before in the context of the stress fraction in Figure 6. Figure 8 is quite similar to Figure 6 in that the Reynolds shear stress is directly correlated to the major turbulence production term $-\overline{u'w'}\partial U/\partial z$ in the TKE transport equation. Sweeps contribute most of the TKE for the large hole size at, and below, the canopy top. The contribution from ejections and sweeps are comparable above the canopy.

[15] Figure 9 shows the quadrant fractions of dissipation rate $\varepsilon^f_{i,H}$. Again, only the in-plane component is considered. In LES, the dissipation rate is calculated in terms of subgrid-scale (SGS) dissipation of kinetic energy $-\tau^{\Delta}_{ij}\tilde{S}_{ij}$, where Δ is the filter size and the tilde represents filtering. The subscripts i and j are the indices for the in-plane components. The SGS dissipation is close to the real dissipation rate when the SGS kinetic energy is assumed to be in equilibrium and Δ is in the inertial range [*Lilly*, 1967; *Meneveau and Katz*, 2000]. The PIV dissipation rate is estimated by fitting a $-5/3$ slope line to the inertial range of the energy spectra obtained from PIV vector maps [*Zhu et al.*, 2007]. Each PIV vector map is categorized according to its $u'w'$ characteristics and spectra are computed from contiguous data points in each vector map and then conditionally averaged. *van Hout et al.* [2007] studied the accuracy of the dissipation rate calculation using spectral fitting in detail by comparing it to the SGS energy flux. The results show that the spectral estimate of the dissipation rate may not be very accurate but it is still of the correct order of magnitude. Because in the present paper we focus on normalized fractions of dissipation, the accuracy in the determination of total dissipation is not overly important. The difference in dissipation rate among the quadrant fractions is much smaller than the differences in the shear stress and TKE. At the canopy top, the quadrant fractions are 20%, 30%, 15%, and 35% at $H = 0$, from quadrant 1 to 4, respectively, while the fractions of the momentum flux and TKE of the two interactions are only around 10%. Inside the canopy, the fraction from outward interactions exceeds that from ejections at any hole size, suggesting that

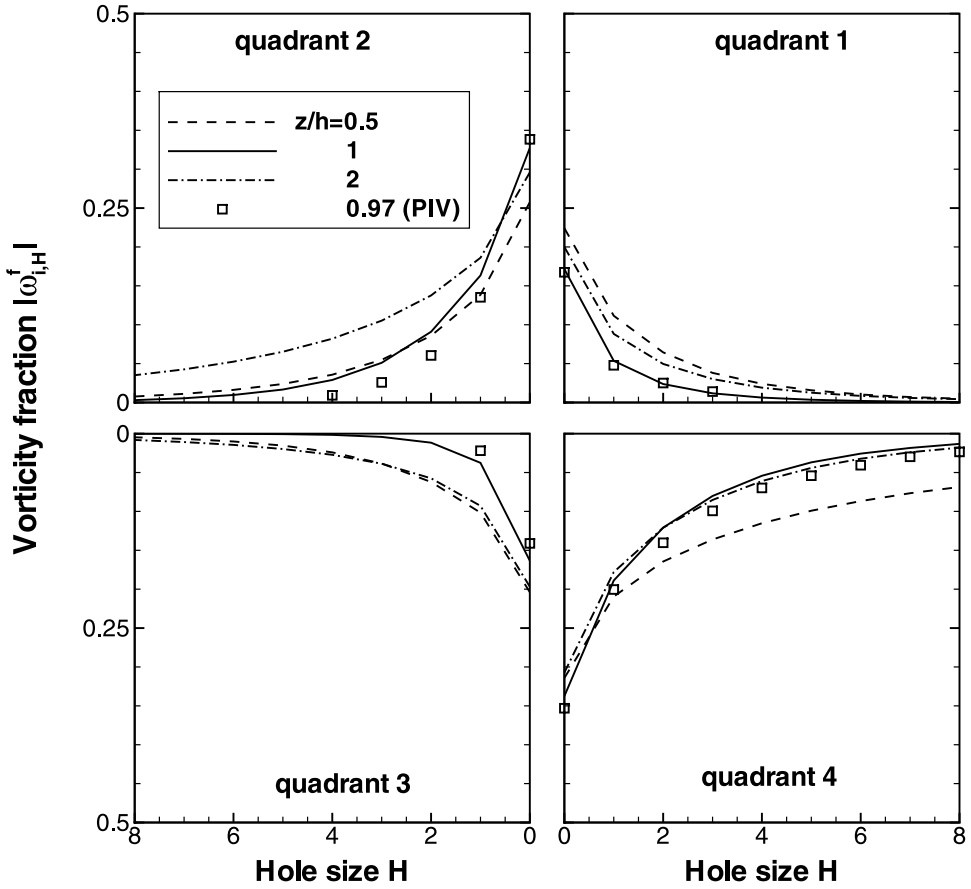

Figure 10. Vorticity fractions $\omega^f_{i,H}$ at three elevations z/h = 0.5, 1, and 2. The PIV data are at z/h = 0.97.

outward interactions play an important role in energy dissipation within the canopy. The field experiment shows that the wake eddies inside the canopy have scales small enough to be approaching the dissipation range [*Zhu et al.*, 2007], and therefore the dissipation rate there relies on the wake deficit velocity (i.e., the instantaneous velocity magnitude in this case). The energy dissipation within and immediately above the canopy is thus expected to have a high rate during the outward interaction events and sweeps. Above the canopy, ejections are still the main contributor to the dissipation rate.

[16] The quadrant fractions of spanwise vorticity magnitude, calculated in terms of the velocity fluctuations, are given in Figure 10. For the PIV experiment, the vorticity is evaluated at the resolution scale (0.56 cm, equivalent to 15 times the Kolmogrov scale), while for the LES, the resolved vorticity at the mesh resolution (10.0 cm) is used. It is still called vorticity here because the mean vorticity magnitude is negligible compared to that of the fluctuating component. The agreement between LES and PIV at the canopy top is quite good. The fractions of ejections and sweeps are comparable at, and below, the canopy top at $H = 0$ and 1. However, sweeps start to dominate at large hole size especially inside the canopy, while ejections dominate above the canopy. The two interactions have similar fractions at all three elevations. Consistent with the shear stress, duration, TKE, and the dissipation rate, the lowest fractions from the two interactions occur at the canopy top, indicating that most turbulence interactions between the atmosphere and the canopy are carried out by sweeps and ejections.

5. Quadrant Magnitude

[17] The normalized quadrant magnitudes of the momentum flux defined in equation (11) are given in Figure 11. In contrast to the fraction plots in Figure 6, the magnitudes of the momentum flux progressively increase with the hole size because of the low duration at the large hole size and the relatively high magnitude of the events. The agreement between LES and PIV at the canopy top is very good. Outward interactions have comparable stress magnitude with ejections throughout the canopy for all hole sizes. Sweeps have a slightly larger stress magnitude above the canopy, and a much larger magnitude inside the canopy for all hole sizes. As for stress fractions, ejections have the largest stress magnitude above the canopy.

[18] In Figure 12 the normalized quadrant magnitudes of TKE are given. Outward interactions and ejections have similar trends and magnitudes throughout the canopy, and inward interactions have a similar trend with slightly lower magnitudes. Sweeps have the largest magnitude at and below the canopy top. The LES prediction of the magnitude of the TKE during sweep events at the canopy top is less than the PIV data. The largest contribution above the canopy is still from ejections.

[19] The LES captures quadrant trends for dissipation rate that are quite similar to those obtained from PIV (see

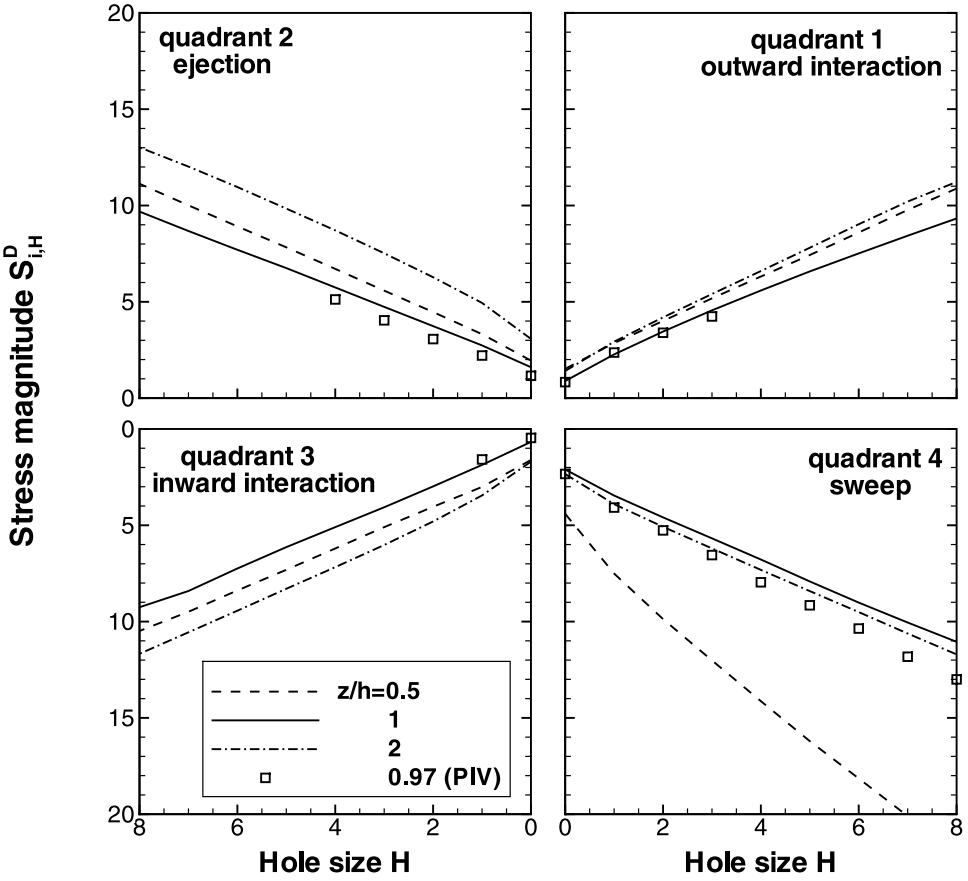

Figure 11. Stress magnitudes $S^D_{i,H}$ at three elevations $z/h = 0.5$, 1, and 2. The PIV data are at $z/h = 0.97$.

Figure 13) for ejections and also other quadrant events at small hole sizes. Differences in magnitudes of sweep and outward interaction quadrants might be attributed to the different methods of estimating the dissipation rate used in the LES and PIV. The low duration at the large hole size may also play a role. During ejection and sweep events, the dissipation rate remains nearly constant for increasing hole size above the canopy, but increases slightly with the hole size during the events of inward interactions. A distinguishing feature in both the LES and PIV results is that the dissipation rate increases greatly with the hole size inside the canopy during outward interaction events. The largest dissipation rate inside the canopy occurs during outward interaction events at all hole sizes as a result of dependency of dissipation rate on wake eddies as discussed in section 4.2. This is different from the shear stress and TKE (Figures 11 and 12), in which sweeps provide the largest contribution.

[20] The quadrant magnitudes of spanwise resolved vorticity are plotted in Figure 14. Note that in contrast to Figure 10, the conditional vorticity magnitude does not decrease with H due to the fact that in Figure 14 the average is normalized by each event duration $D_{i,H}$. The duration decreases at higher H since fewer events occur for increasing H (see Figure 7). Outward interactions produce the largest vorticity magnitude at the canopy top, progressively increasing with the quadrant hole size, similar to the dissipation rate. Sweeps also produce larger vorticity magnitude than ejections and inward interactions at, and below, the canopy top, suggesting that the high-speed flow ($u' > 0$) is more efficient in generating the vorticity than the low-speed flow ($u' < 0$) within the canopy. The resemblance between Figures 14 and Figure 13 suggests a strong relationship between the dissipation rate and the vorticity, while little correlation is seen between the vorticity and the shear stress (see Figures 14 and 11). This is not surprising, as vorticity and the dissipation rate are primarily governed by the small-scale flow structures and the shear stress is basically governed by the large scales. The strong correlation between vorticity and dissipation rate was also observed by *van Hout et al.* [2007].

6. Summary and Conclusions

[21] A quadrant analysis was employed to investigate the accuracy of LES to predict detailed statistical features of coherent structures. The quadrant-hole analysis technique was used to study the effects of coherent structures on the vertical momentum flux, TKE, time duration, dissipation rate of kinetic energy, and vorticity magnitude. The mean strength of coherent structure signals was also examined by taking into account the effect of the event duration on the event magnitude. With a few exceptions, there is good agreement between the quadrant-hole analysis results from LES and the PIV data, confirming the reliability of LES to simulate flow in vegetative canopies. Since the PIV data used here are only available at the top of the canopy, further experimental measurements need to be carried out at additional selected elevations inside and above the canopy for a

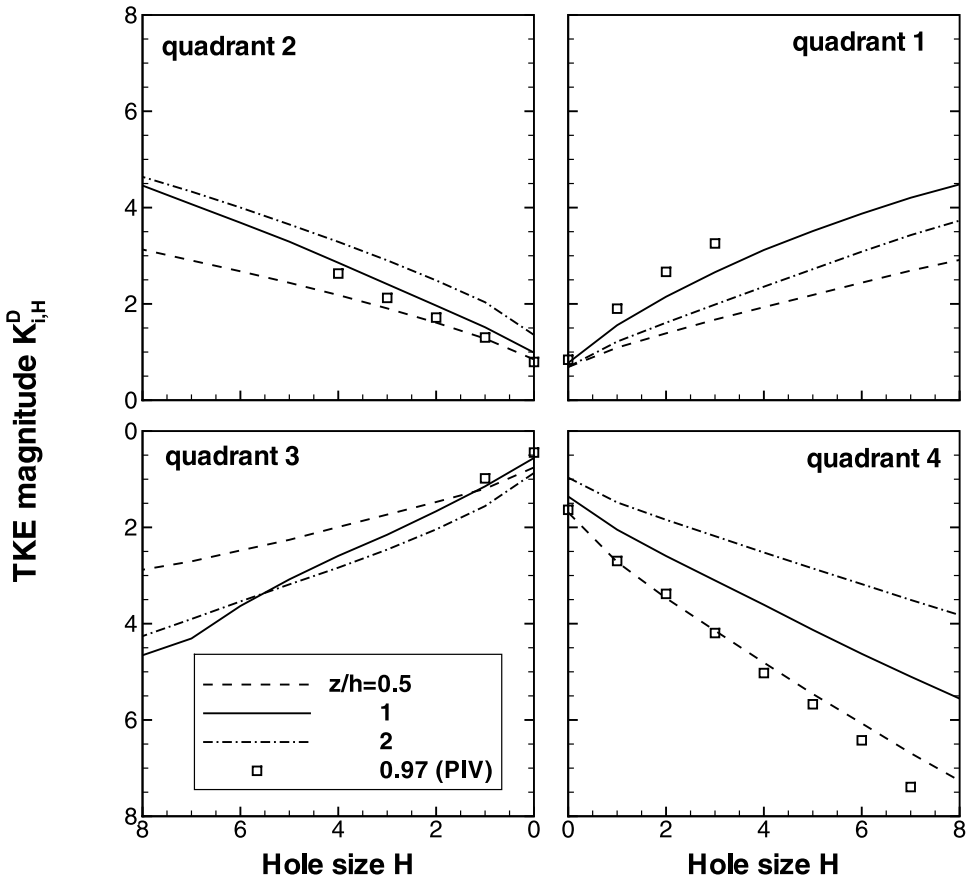

Figure 12. TKE magnitudes $K^D_{i,H}$ at three elevations z/h = 0.5, 1, and 2. The PIV data are at z/h = 0.97.

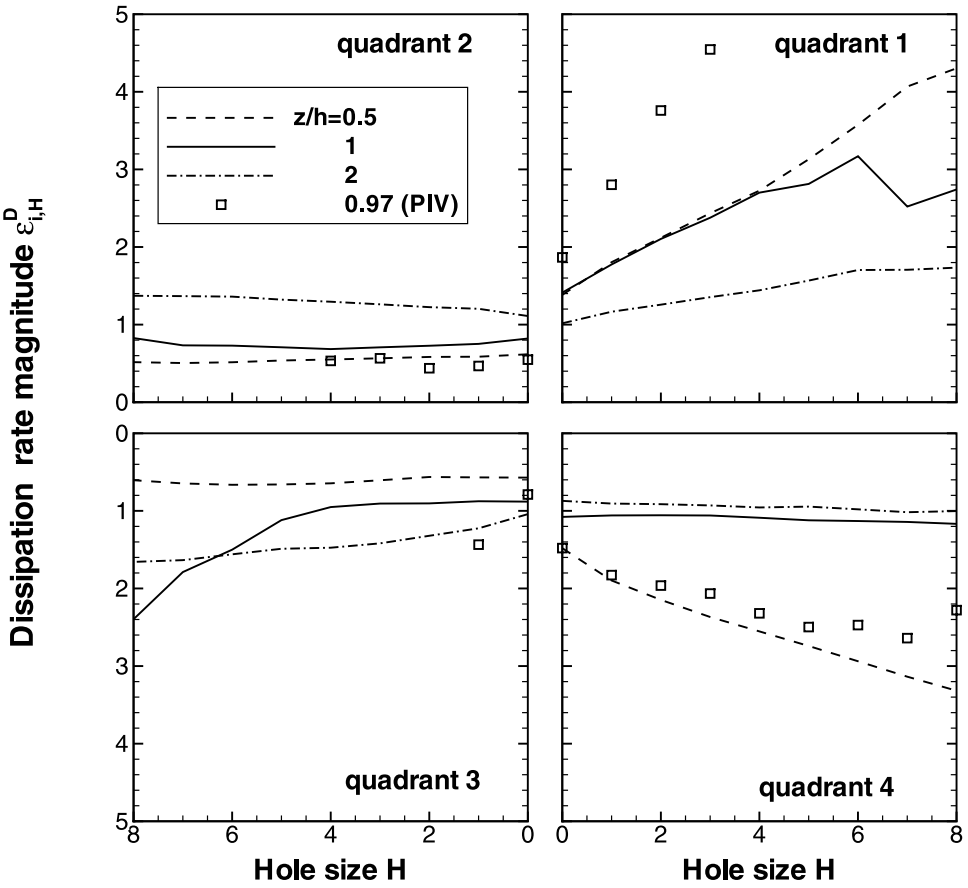

Figure 13. Dissipation rate magnitudes $\varepsilon^D_{i,H}$ at three elevations z/h = 0.5, 1, and 2. The PIV data are at z/h = 0.97.

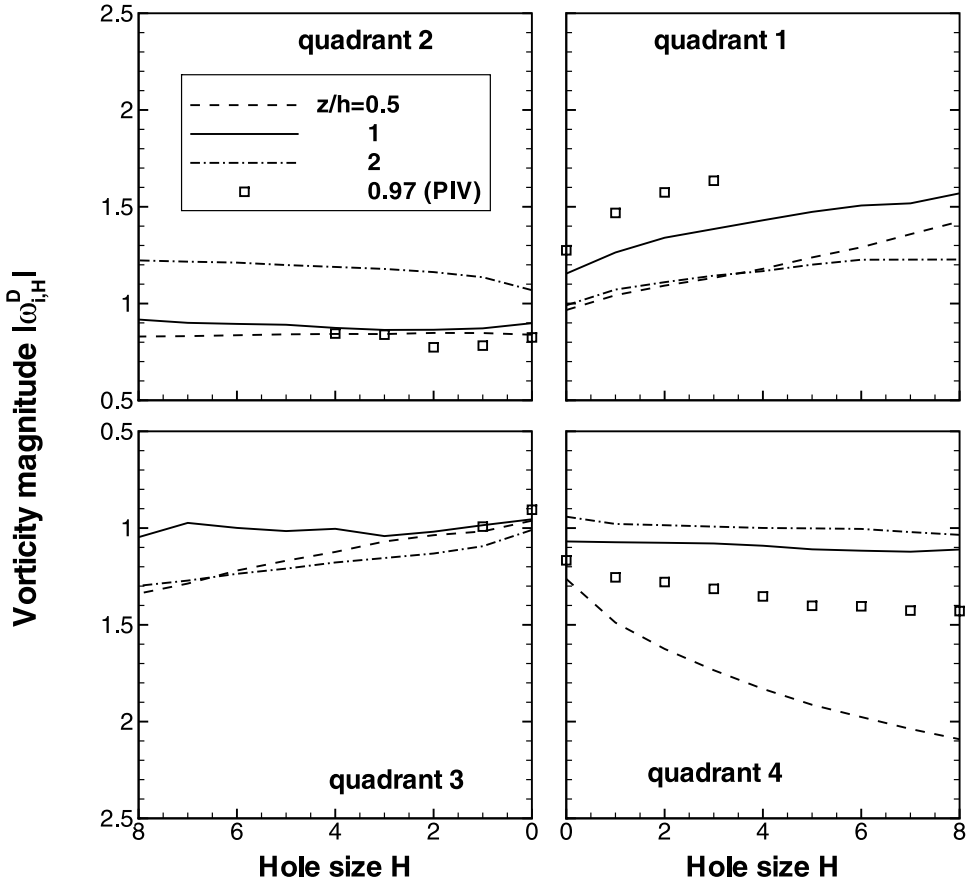

Figure 14. Resolved vorticity magnitudes $\omega^D_{i,H}$ at three elevations z/h = 0.5, 1, and 2. The PIV data are at z/h = 0.97.

more complete comparison to the LES results. Around the canopy top, ejections are the most frequently occurring events (longest time fraction) while sweeps contribute the most to the vertical momentum flux (largest fraction). The events of outward and inward interactions have the shortest time fraction and the smallest fractions of the shear stress and TKE, especially at the canopy top, indicating that the momentum and kinetic energy transfer between the atmosphere and the canopy is mostly carried by ejection and sweep events. However, the fractional contributions to the vorticity (at LES and PIV resolutions) and dissipation rate from the two interactions are significant. It was also found that significant fractions of the vertical momentum flux are transported at high values of the hole size, indicating that much of the momentum flux is transported during periods of strong turbulent events occupying in a small fraction of time.

[22] The magnitudes of the vorticity and the dissipation rate are the highest during the rare events of outward interactions at the canopy top. The resemblance between dissipation rate and vorticity magnitudes is noted, indicating a strong correlation between these two flow quantities as revealed by *Zhu et al.* [2007], and consistent with the fact that dissipation and vorticity are mainly governed by the small-scale flow structures. On the other hand, the momentum flux is governed by the large scales, and it is not surprising to see that there is little correlation observed between the shear stress and the vorticity. The good overall agreement between quadrant analysis results from LES and PIV supports the reliability of using LES for fundamental studies of canopy turbulence, not just for bulk averaged quantities but also for high-order statistical quantities indicative of coherent structure behavior.

[23] **Acknowledgments.** This study was partially supported by the National Science Foundation Biocomplexicity program under grant BES-0119903.

References

Albertson, J. D., and M. B. Parlange (1999a), Natural integration of scalar fluxes from complex terrain, *Adv. Water Resour.*, *23*, 239–252.

Albertson, J. D., and M. B. Parlange (1999b), Surface length-scales and shear stress: Implications for land-atmosphere interaction over complex terrain, *Water Resour. Res.*, *35*, 2121–2132.

Alfredsson, P. H., and A. V. Johansson (1984), On the detection of turbulence-generating events, *J. Fluid Mech.*, *139*, 325–345.

Andradottir, H. O., and H. M. Nepf (2001), Impact of exchange flows on wetland flushing, *Water Resour. Res.*, *37*, 3265–3273.

Antonia, R. A. (1981), Conditional sampling in turbulence measurement, *Annu. Rev. Fluid Mech.*, *13*, 131–156.

Aubertine, C. D., and J. K. Eaton (2005), Turbulent development in a non-equlibrium turbulent boundary layer with mild adverse pressure gradient, *J. Fluid Mech.*, *532*, 345–364.

Baldocchi, D. D., and T. P. Meyers (1988), Turbulence structures in a deciduous forest, *Boundary Layer Meteorol.*, *43*, 345–364.

Blackwelder, R. F., and R. E. Kaplan (1976), On the wall structure of the turbulent boundary layer, *J. Fluid Mech.*, *76*, 89–112.

Bou-Zeid, E., C. Meneveau, and M. B. Parlange (2004), Large-eddy simulation of neutral atmospheric boundary layer flow over heterogeneous surfaces: Blending height and effective surface roughness, *Water Resour. Res.*, *40*, W02505, doi:10.1029/2003WR002475.

Bou-Zeid, E., C. Meneveau, and M. B. Parlange (2005), A scale-dependent Lagrangian dynamic model for large eddy simulation of complex turbulent flows, *Phys. Fluids*, *17*, 025105.

Cava, D., G. G. Katul, A. Scrimieri, D. Poggi, A. Cescatti, and U. Giostra (2006), Buoyancy and the sensible heat flux budget within dense canopies, *Boundary Layer Meteorol.*, *118*, 217–240.

Charnay, G., J. Mathieu, and G. Comte-Bellot (1976), Response of a turbulent boundary layer to random fluctuations in the external stream, *Phys. Fluids*, *19*, 1261–1272.

Chu, D. C., and G. E. M. Karniadakis (1993), A direct numerical-simulation of laminar and turbulent-flow over riblet-mounted surfaces, *J. Fluid Mech.*, *250*, 1–42.

Farge, M. (1992), Wavelet transforms and their applications to turbulence, *Annu. Rev. Fluid Mech.*, *24*, 395–458.

Finnigan, J. (2000), Turbulence in plant canopies, *Annu. Rev. Fluid Mech.*, *32*, 519–571.

Finnigan, J. J. (1979), Turbulence in waving wheat: I. Mean statistics and honami, *Boundary Layer Meteorol.*, *16*, 181–211.

Finnigan, J. J., and R. H. Shaw (2000), A wind-tunnel study of air flow in waving wheat: An EOF analysis of the structure of the large-eddy motion, *Boundary Layer Meteorol.*, *96*, 211–255.

Gardiner, B. A. (1994), Wind and wind forces in a plantation spruce forest, *Boundary Layer Meteorol.*, *67*, 161–186.

Ghisalberti, M., and H. M. Nepf (2004), The limited growth of vegetated shear layers, *Water Resour. Res.*, *40*, W07502, doi:10.1029/2003WR002776.

Katul, G., D. Poggi, D. Cava, and J. Finnigan (2006), The relative importance of ejections and sweeps to momentum transfer in the atmospheric boundary layer, *Boundary Layer Meteorol.*, *102*, 367–375.

Katul, G. G., and M. B. Parlange (1994), On the active-role of temperature in surface-layer turbulence, *J. Atmos. Sci.*, *51*, 2181–2195.

Kim, S. W., S. U. Park, and C.-H. Moeng (2003), Entrainment processes in the convective boundary layer with varying wind shear, *Boundary Layer Meteorol.*, *108*, 221–245.

Lilly, D. K. (1967), The representation of small-scale turbulence in numerical simulation experiments, in *Proceedings of IBM Scientific Computing Symposium on Environmental Sciences*, pp. 195–210, IBM Data Process. Div., White Plains, N. Y.

Lu, S., and W. W. Willmarth (1973), Measurements of the structure of the Reynolds stress in a turbulent boundary layer, *J. Fluid Mech.*, *60*, 481–511.

Mahrt, L. (1991), Eddy asymmetry in the sheared heated boundary-layer, *J. Atmos. Sci.*, *48*, 472–492.

Marsh, B. J., C. J. Wood, B. A. Gardiner, and R. E. Belcher (2001), Conditional sampling of forest canopy gusts, *Boundary Layer Meteorol.*, *102*, 225–251.

Mason, P. J. (1994), Large eddy simulation: A critical review of the technique, *Q. J. R. Meteorol. Soc.*, *120*, 1–26.

Meneveau, C. (1991), Analysis of turbulence in the orthonormal wavelet representation, *J. Fluid Mech.*, *232*, 469–520.

Meneveau, C., and J. Katz (2000), Scale-invariance and turbulence models for large-eddy simulation, *Annu. Rev. Fluid Mech.*, *32*, 1–32.

Mokhtarzadeh-Dehghan, M. R., and Y. M. Yuan (2002), Measurements of turbulence quantities and bursting period in developing turbulent boundary layers on the concave and convex walls of a 90 degrees square bend, *Exp. Thermal Fluid Sci.*, *27*, 59–75.

Orszag, S. S. (1970), Transform method for calculation of vector coupled sums: Application to the spectral form of vorticity equation, *J. Atmos. Sci.*, *27*, 890–895.

Poggi, D., G. G. Katul, and J. D. Albertson (2004a), Momentum transfer and turbulent kinetic energy budgets within a dense model canopy, *Boundary Layer Meteorol.*, *111*, 589–614.

Poggi, D., A. Porporato, L. Ridolfi, J. D. Albertson, and G. G. Katul (2004b), The effect of vegetation density on canopy sub-layer turbulence, *Boundary Layer Meteorol.*, *111*, 565–587.

Porporato, A. (1999), Conditional sampling and state space reconstruction, *Exp. Fluids*, *26*, 441–450.

Porté-Agel, F., C. Meneveau, and M. B. Parlange (2000), A scale-dependent dynamic model for large-eddy simulation: Application to a neutral atmospheric boundary layer, *J. Fluid Mech.*, *415*, 261–284.

Priyadarshana, P. J. A., and J. C. Klewicki (2004), Study of the motions contributing to the Reynolds stress in high and low Reynolds number turbulent boundary layers, *Phys. Fluids*, *16*, 4586–4600.

Raupach, M. R. (1981), Conditionial statistics of Reynolds stress in rough-wall and smooth-wall turbulent boundary layers, *J. Fluid Mech.*, *108*, 363–382.

Raupach, M. R., and A. S. Thom (1981), Turbulence in and above plant canopies, *Annu. Rev. Fluid Mech.*, *13*, 97–129.

Raupach, M. R., P. A. Coppin, and B. J. Legg (1986), Experiments on scalar dispersion within a model plant canopy. Part I: The turbulence structure, *Boundary Layer Meteorol.*, *35*, 21–52.

Raupach, M. R., R. A. Antonia, and S. Rajagopalan (1991), Rough-wall turbulent boundary layer, *Appl. Mech. Rev.*, *44*, 1–25.

Robinson, S. K. (1991), Coherent motions in the turbulent boundary layer, *Annu. Rev. Fluid Mech.*, *23*, 601–639.

Shaw, R. H., and U. Schumann (1992), Large-eddy simulation of turbulent flow above and within a forest, *Boundary Layer Meteorol.*, *61*, 47–64.

Shaw, R. H., J. Tavangar, and D. P. Ward (1983), Structure of the Reynolds stress in a canopy layer, *J. Clim. Appl. Meteorol.*, *22*, 1922–1931.

Shen, S., and M. Y. Leclerc (1997), Modelling the turbulence structure in the canopy layer, *Agric. For. Meteorol.*, *87*, 3–25.

Sreenivasan, K. R., R. A. Antonia, and S. E. Stephenson (1978), Conditional measurements in a heated axisymmetric turbulent mixing layer, *AIAA J.*, *16*, 869–870.

Su, H.-B., R. H. Shaw, K. T. Paw U, C.-H. Moeng, and P. P. Sullivan (1998), Turbulent statistics of neutrally stratified flow within and above a sparse forest from large-eddy simulation and field observations, *Boundary Layer Meteorol.*, *88*, 363–397.

Szilagyi, J., M. B. Parlange, G. G. Katul, and J. D. Albertson (1999), An objective method for determining principal time scales of coherent eddy structures using orthonormal wavelets, *Adv. Water Resour.*, *22*, 561–566.

van Hout, R., W. Zhu, L. Luznik, J. Katz, J. Kleissl, and M. B. Parlange (2007), PIV measurements in the atmospheric boundary layer within and above a mature corn canopy. Part A: Statistics and energy flux, *J. Atmos. Sci.*, in press.

Wallace, J. M., H. Eckelmann, and R. S. Brodkey (1972), Structure of the Reynolds stress near the wall, *J. Fluid Mech.*, *54*, 65–92.

Watanabe, T. (2004), Large-eddy simulation of coherent turbulence structures associated with scalar ramps over plant canopies, *Boundary Layer Meteorol.*, *112*, 307–341.

Weir, A. D., and P. Bradshaw (1979), The interaction of two parallel free shear layers, paper presented at the Second Symposium on Turbulent Shear Flows, Imperial College London, London.

Willmarth, W. W., and S. S. Lu (1972), Structure of the Reynolds stress near the wall, *J. Fluid Mech.*, *54*, 65–92.

Yue, W., C. Meneveau, M. B. Parlange, W. Zhu, R. van Hout, and J. Katz (2007), Turbulence structures within and above a corn canopy, using field- and plant-scale representations, *Boundary Layer Meteorol.*, in press.

Zhu, W., R. van Hout, and J. Katz (2007), PIV measurements in the atmospheric boundary layer within and above a mature corn canopy. Part B: Quadrant-hole analysis, *J. Atmos. Sci.*, in press.

J. Katz, C. Meneveau, and W. Zhu, Department of Mechanical Engineering, Johns Hopkins University, 3400 North Charles Street, Baltimore, MD 21218, USA. (meneveau@jhu.edu)

M. B. Parlange, School of Architecture, Civil and Environmental Engineering, Ecole Polytechniqul Federale de Lausanne, Lausanne, CH-1015, Switzerland. (marc.parlange@epfl.ch)

W. Yue, Department of Geography and Environmental Engineering, Johns Hopkins University, 3400 North Charles Street, Baltimore, MD 21218, USA. (yue@jhu.edu)

R. van Hout, Faculty of Mechanical Engineering, Technion-IIT, Technion city, Haifa 32000, Israel. (rene@tx.technion.ac.il)